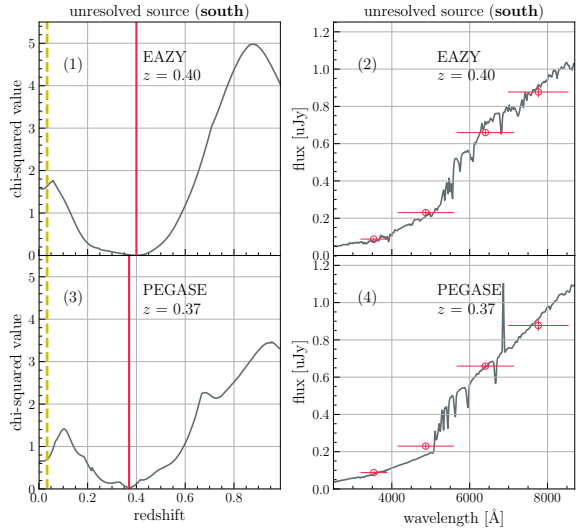

a

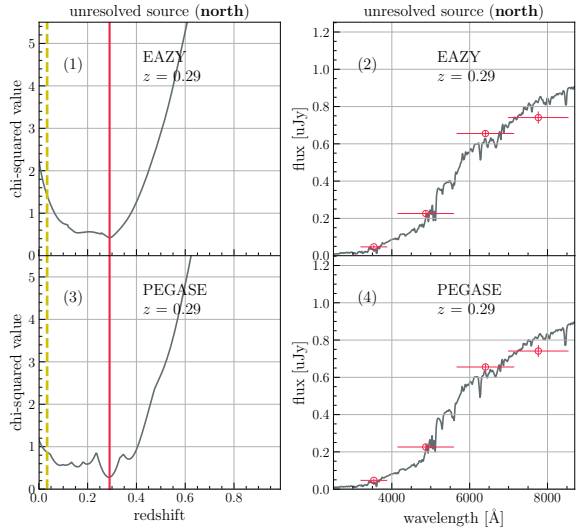

b

Figure 6. The SED-fitting results of the two unresolved (point-like) sources appearing in the residual images after subtracting the model images of the dry merger (Satsuki and Mei). The results of the southern and northern sources are presented in panel (a) and (b), respectively. For each panel, the sub-panels (1) and (2) show the chi-squared values of the fit for a given redshift using the EAZY template and the best-fit SED with observed fluxes at *i*-, *r*-, *g*- and *u*-band overlaid as red circles, respectively. The corresponding plots using the PÉGASE template are shown in sub-panels (3) and (4). The red solid vertical lines in sub-panels (1) and (3) mark the redshift of minimum chi-squared value. The redshift of our target is indicated by yellow dashed lines.

3.2.2. *Interaction Features*

If Totoro is indeed a separate galaxy, it may possess another tidal tail on the other side of the blob (i.e., as opposed to the ones that connect the Totoro and Satsuki), but such tail(s) would not be seen by MaNGA due to the limited FoV. Figure 7 shows the new wide-field Hα image taken from the SAO RAS 6-m telescope. The new Hα map has a sensitivity comparable to that of MaNGA, but the FoV is $\sim$ 10 times larger. For comparison, Figure 7a zooms in to the region of the MaNGA hexagonal FoV. The new Hα image globally resembles that of the MaNGA Hα in Figure 1a, but shows finer structures thanks to higher spatial resolution.

A zoom-out view of the region of interest is displayed in Figure 7b. There are several Hα knots beyond the MaNGA FoV towards the east. These are background galaxies or foreground stars. It is clear that there is no hint of Hα emission extending beyond the MaNGA FoV at the opposite side Totoro. Quantitatively, we can estimate the possible missing flux of MaNGA by comparing the Hα flux related with Totoro from the two observations. The total Hα luminosity of Totoro and the surrounding $\sim$15″ ($\sim$ 9 kpc) region outside of the MaNGA FoV (blue circle in Figure 7b) is 6.5×10^{39} erg s^{-1}. The total Hα luminosity of Totoro measured by MaNGA is 5.9×10^{39} erg s^{-1}. Therefore the possible missing flux of Totoro due to limited MaNGA FoV is no larger than 10%. Accordingly, the scenario of a separate galaxy appears less likely unless the tidal tail(s) develop at only one side of a galaxy. Such cases are relatively rare, though not impossible (e.g., Arp 173, Arp188, and Arp 273), depending on the stage of the interaction and the projected orientation on the sky (e.g., Mihos 2004; Struck & Smith 2012). However, the low gas velocity provides additional support against a merger scenario (Figure 3c and 3d).

On the other hand, it is possible that Totoro is a completely disrupted dwarf galaxy. The averaged surface brightness of Totoro has an upper limit of $\sim$ 27 mag arcsec^{-2} (Table 3). It would be classified as a dwarf low-surface-brightness galaxy (LSB; $>$ 23 mag arcsec^{-2}) if it is a galaxy. In the next section, we compare the star formation and cold gas properties of Totoro with other galaxy populations, including LSBs.

As a side note, the nearby galaxy NGC 6338 is encompassed by the wide-field Hα observation. Figure 7c shows the Hα image of NGC 6338. There is no strong filaments or bridge linking NGC 6338 and VII Zw 700, presumably because the two are very separate entities (with projected separation of $\sim$ 42 kpc and $\sim$ 1400 km s^{-1} difference in line of sight velocity), but there is a bit more Hα emission between galaxies than the rest of the regions in the plotted area. The Hα emission of NGC 6338 is characteristic of three previously-reported filaments in the southeast and northwest quadrants. The Hα intensity contours of 0.035 and 0.09×10^{-16} erg s^{-1} cm^{-2} are overplotted to highlight the asymmetric fila-

ments. We also refer the reader to Martel et al. (2004) and O'Sullivan et al. (2019) for higher-resolution Hα images of NGC 6338 and Gomes et al. (2016) for optical IFS data analysis of NGC 6338.

3.2.3. *M_{H_2}-SFR Relation of Galaxies*

Another way to constrain the origin of Totoro using data in hand is to look into the question of whether Totoro shares similar gas and star formation properties with nearby galaxies. This could not be concluded in Paper I due to the lack of cold gas data. Figure 8 compares the star formation rate (SFR) and molecular gas mass (M_{H_2}) of Totoro with other galaxy populations. The plot resembles the Kennicutt-Schmidt relation (Kennicutt 1989) assuming that the molecular gas and star-forming regions coexist. The galaxy data include nearby LSBs (O'Neil et al. 2003; Matthews et al. 2005; Cao et al. 2017), nearby star-forming (sSFR $> 10^{-11}$ yr^{-1}) and quiescent (sSFR $< 10^{-11}$ yr^{-1}) galaxies (Saintonge et al. 2017).

The total Hα luminosity of Totoro (including the connecting arms; $\sim$48.1 kpc^2 area in total) is converted to SFR using the calibration of

$$\frac{\mathrm{SFR}}{[\mathrm{M_\odot\,yr^{-1}}]} = 7.9 \times 10^{42} \frac{L_{\mathrm{H}\alpha}}{[\mathrm{erg\,s^{-1}}]} \quad (1)$$

(Kennicutt 1998), where $L_{\mathrm{H}\alpha}$ is Hα luminosity. This yields a SFR of 0.047 M$_\odot$ yr^{-1}. Here we assume all of the Hα results from star formation, but this is unlikely to be the case as BPT diagnostics indicate a composite nature, LI(N)ER-HII mix excitation, for Totoro (Paper I). Therefore the derived SFR is an upper limit.

The total molecular gas mass of Totoro traced by CO is computed using

$$\frac{M_{H_2}}{[\mathrm{M_\odot}]} = 1.05 \times 10^4 \frac{X_{\mathrm{CO}}}{[2 \times 10^{20}\,\mathrm{cm^{-2}(K\,km\,s^{-1})^{-1}}]} \frac{S_{\mathrm{CO}}\Delta v}{[\mathrm{Jy\,km\,s^{-1}}]} \frac{D_{\mathrm{L}}^2}{[\mathrm{Mpc}]} (1+z)^{-1} \quad (2)$$

,where X_{CO}, $S_{\mathrm{CO}}\Delta\nu$, D_{L} are CO-to-H$_2$ conversion factor, integrated line flux density, and luminosity distance, respectively (Bolatto et al. 2013). We adopt a Galactic X_{CO} of 2×10^{20} cm^{-2} (K km s^{-1})$^{-1}$ (Bolatto et al. 2013). The derived M_{H_2}[11] of Totoro is (2.1$\pm$0.1) $\times$ 10^8 M$_\odot$. Note that the uncertainty due to different methodologies to derived the Galactic X_{CO} is $\sim$ 30% (Bolatto et al. 2013).

In addition to CO, the gaseous column density N_{H_2} (and M_{H_2}) also follows from the amount of extinction A_{V}, which can be derived from the MaNGA Hα and Hβ data. For reference, the mean A_{V} across Totoro is $\sim$ 0.5 mag. The conversion from extinction to H$_2$ column density depends on the medium (Bohlin et al. 1978; Evans et al. 2009):

$$\frac{N(\mathrm{H_2})}{[\mathrm{cm^{-2}}]} = 6.9 \times 10^{20} \frac{A_{\mathrm{v}}}{[\mathrm{mag}]}\,(\mathrm{molecular\,cloud}) \quad (3)$$

$$= 9.4 \times 10^{20} \frac{A_{\mathrm{v}}}{[\mathrm{mag}]}\,(\mathrm{diffuse\,ISM}). \quad (4)$$

These yield a M_{H_2} of $\sim$ 1.9 $\times$ 10^8 and $\sim$ 2.5 $\times$ 10^8 M$_\odot$ assuming molecular-cloud- (Equation 3) and diffuse-ISM-type (Equation 4) medium, respectively. The three M_{H_2} derived using radio and optical measurements agree well with each other. The H$_2$ mass derived from CO is used for the discussion in the rest of the paper.

Although only upper limits could be achieved for many LSB objects, they largely follow the trend established by star forming galaxies towards the lower end in both M_{H_2} and SFR axes, consistent with the finding of McGaugh et al. (2017). On the other hand, quiescent galaxies, mostly early types, have lower SFR for a given M_{H_2} and a lower CO detection rate than that of star-forming galaxies (see also Calette et al. 2018). Due to the low SFR, Totoro deviates from the SFR-M_{H_2} relation formed by LSBs and star-forming galaxies and appears to overlap with quiescent galaxies.

The Hα emission in quiescent galaxies is dominated by LI(N)ER excitation (Hsieh et al. 2017; Pan et al. 2018). In the LI(N)ER regions of quiescent galaxies, surface density of Hα luminosity ($\Sigma_{\mathrm{H}\alpha}$) is found to be tightly correlated with underlying Σ_* (Hsieh et al. 2017), in which the Hα are primarily powered by the hot, evolved stars rather than recent star formation. BPT diagnostics suggest that Totoro is powered by a composite

[11] We should note that the value of M_{H_2} depends on the choice of X_{CO}. We may overestimate M_{H_2} by $\sim$ 30% to a factor of a few if the metallicity of Totoro is indeed higher than the solar metallicity by $\sim$ 0.3 dex as discussed in the Introduction (Bolatto et al. 2013). Vantyghem et al. (2017) use the optical thin ^{13}CO(3-2) emission line to estimate X_{CO} of the BCG of the cooling-core cluster RXJ0821+0752, finding a X_{CO} of a factor of two lower than the Galactic (our adopted) value. However, this is within the object-to-object scatter from extragalactic sources, and based on several assumptions such as isotopic abundance ratio and excitation line ratios. Statistical analysis is necessary in order to constrain the X_{CO} in BCGs.

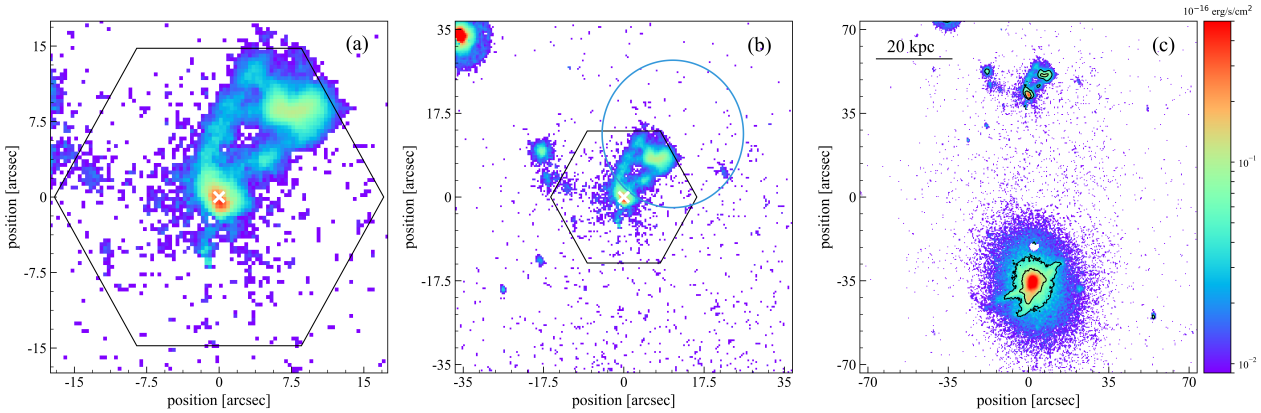

Figure 7. New, wide-field narrow-band Hα image taken from the SAO RAS 6-m telescope. (a) A zoom-in to the region of the MaNGA observation with the MaNGA hexagonal bundle FoV overlaid. The color scale is the same as in Figure 1a. The nucleus of Satsuki is marked by a cross. (b) A zoom-out view of the region of interest. It is clear that there is no hint of tidal feature extending beyond the MaNGA FoV. Quantitatively, the total Hα luminosity in the blue circle ($15''$ or ~ 9 kpc in radius) is only $\sim 10\%$ higher than the luminosity of Totoro measured by MaNGA, therefore the possible missing flux that is associated with Totoro due to the small MaNGA FoV is at most 10%. (c) The Hα image of NGC 6338 and our target. The two contours correspond to 0.035 and 0.09 $\times$ 10^{-16} erg s^{-1} cm^{-2}, respectively.

(LI(N)ER-HII mix) mechanism (Paper I). If Totoro is analogous to a LI(N)ER region in quiescent (early-type) galaxies, the average $\Sigma_{\rm H\alpha}$ of Totoro corresponds to a Σ_* of $\sim 7 \times 10^8$ M$_\odot$ kpc^{-2} according to the "resolved LI(N)ER sequence" of quiescent galaxies reported by Hsieh et al. (2017). The predicted Σ_* is higher than the mass of Satsuki's stellar halo by a factor of 3 – 5; however, there is no distinct stellar counterpart at the location of Totoro. For this reason, in spite of the overlap in Figure 8, Totoro is not analogous to the LI(N)ER region in quiescent galaxies. Lastly, we should note that if the true global SFR of Totoro is considerably lower than the upper limit, Totoro would fall below the main cloud of data points of quiescent galaxies.

As a whole, Totoro is unlikely to be consistent with nearby normal star-forming, early-type, and low-surface-brightness galaxies in terms of the Kennicutt-Schmidt relation and the resolved LI(N)ER sequence. In addition, it is worth noting that the average $A_{\rm V}$ of Totoro corresponds to a SFR surface density ($\Sigma_{\rm SFR}$) at least 6 times higher than the observed upper limit based on the local $A_{\rm V}$-$\Sigma_{\rm SFR}$ relation derived from MaNGA galaxies (Li et al. 2019). Generally speaking, the dust and star formation relation (if any) of Totoro is also dissimilar to that of star-forming regions in nearby galaxies even when the systematic dependencies on other physical properties (e.g., metallicity) are considered.

While LSBs have been studied for decades, recently, van Dokkum et al. (2015) have identified a new class of LSBs in the Coma cluster, ultra-diffuse galaxies (UDGs). These UDGs have a surface brightness as low as > 24.5 mag arcsec^{-2}, but their sizes are similar to those of L^* galaxies. It is not clear how UDGs were formed. One possible scenario is that UDGs are failed massive galaxies, which lost their gas at high redshift by ram-pressure stripping or other effects after forming their first generation of stars (van Dokkum et al. 2015; Yozin, & Bekki 2015). Our finding of a large molecular gas reservoir appears in direct conflict with this scenario.

On the other hand, several studies suggest that UDGs are extended dwarf galaxies. Some simulations predict them to be rapidly rotating (Amorisco, & Loeb 2016). Di Cintio et al. (2017) suggest that the extended sizes of UDGs are the consequence of strong gas outflows driven by starbursts. However, the SFR of Totoro is extremely low and the system is not rotating. Altogether, there is no evidence in our data to support Totoro as an UDG.

In summary, the newly obtained CO, Hα, and u-band data allow us to better constrain the nature of Totoro; however, combining the results in Section 3.2, we argue that Totoro is unlikely to be a separate galaxy interacting with the dry merger (Satsuki and Mei). The reasons include the lack of stellar counterpart and tidal features and the different star formation, ionized and cold gas, and dust properties (i.e., $M_{\rm H_2}$-SFR, Σ_*-$\Sigma_{\rm H\alpha}$, and $A_{\rm V}$-$\Sigma_{\rm SFR}$ relations and gas kinematics) from that of a variety of nearby galaxy populations (i.e., star-forming and quiescent galaxies, LSBs, and UDGs).

3.3. *AGN-driven Activity*

3.3.1. *Multi-wavelength Nuclear Characteristics*

Radio. A possible origin of Totoro is gas that is photoionized by X-ray emission from a misaligned blazar at the core of Satsuki. A blazar is a sub-class of radio-

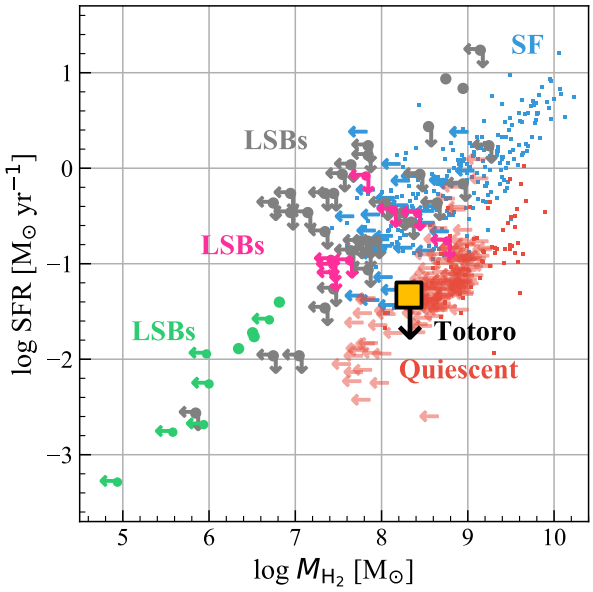

Figure 8. Star formation rate versus H_2 mass. The orange square is Totoro from this work. The gray, green, and magenta symbols are LSBs measurements from O'Neil et al. (2003), Matthews et al. (2005), and Cao et al. (2017), respectively. Objects with solid detection in CO lines are shown with squares. An arrow indicates that only an upper limit was found. Blue and red squares are nearby star-forming (sSFR $> 10^{-11}$ yr^{-1}) and quiescent (sSFR $< 10^{-11}$ yr^{-1}) galaxies taken from the xCOLD GASS survey (Saintonge et al. 2017). In all cases a conversion factor of 2.0×10^{20} cm^{-2} (K km s^{-1})$^{-1}$ (Bolatto et al. 2013, the uncertainty of the conversion factor is $\sim 30\%$) is used to allow ready comparison between the studies.

loud AGN which is characterized by one-sided jet structure (Urry & Padovani 1995). However, blazars invariably have bright compact radio cores, whereas no detection at 1.4 GHz is found for Satsuki (Wang et al. 2019; O'Sullivan et al. 2019) and there is only marginal detection at 5 GHz (Paper I). For these reasons, a blazar is a very unlikely scenario for Totoro.

Optical. The Hα equivalent width (EW) is < 3Å across the entire Hα-emitting region and the EW does not present a rise towards the center of Satsuki. The Hα velocity dispersion does not present a central peak either (Paper I). Moreover, the Hα luminosity of Satsuki follows the continuum emission, i.e., does not present a central peak emission with stronger intensities that follows an r^{-2} or lower decline from the center (Singh et al. 2013). Therefore, Satsuki presents a lack of optical characteristics of a strong AGN.

X-ray. A comprehensive study of the X-ray emission of the region based on *Chandra* and *XMM-Newton* data has been reported recently by O'Sullivan et al. (2019). Figure 9a shows the *Chandra* X-ray image of the NGC 6338 group taken from O'Sullivan et al. (2019). X-ray and galaxy velocity studies have shown the group to be a high-velocity near head-on merger (Wang et al. 2019), with the two group cores visible as bright clumps of X-ray emission with trailing X-ray tails. The northern and southern clumps are respectively associated with VII Zw 700 and NGC 6338. Figure 9b zooms in to the MaNGA observed region. The northern X-ray clump, around Satsuki, is dominated by a bar of X-ray emission extending roughly southeast-northwest. The clump and bar are centered somewhat to the north of the optical centroid of Satsuki, and the bar is made up of three X-ray knots whose intensities progressively decrease from the western end. The nuclei of Satsuki and Mei are not correlated with the brightest X-ray emission (see also Wang et al. 2019). Nonetheless, after subtracting the overall surface brightness distribution, there is a hint of excess X-ray emission at the position of the nuclei of Satsuki and Mei (see O'Sullivan et al. 2019 for the construction of the overall surface brightness distribution). X-ray luminosities of 4.17×10^{39} erg s^{-1} for the nucleus of Satsuki and $\leqslant 2.5 \times 10^{38}$ erg s^{-1} for Mei are reported (O'Sullivan et al. 2019). The values suggest that there are no strong X-ray AGN in Satsuki or Mei or the AGNs are fading. For reference, the X-ray luminosity of Totoro is $(4.4 \pm 0.2) \times 10^{40}$ erg s^{-1}.

3.3.2. *Gas Ejected by AGN*

All in all, the multi-wavelength data show no direct evidence for an active ongoing AGN in Satsuki. However, it is known that the AGN luminosity can vary over timescales as short as 10^5 years. Thus, we still cannot rule out the possibility of a recent AGN outflow. AGN-driven extended outflows are detected in multiple phases, including ionized gas and many molecular lines (Roberts-Borsani 2020, and references therein). Even though the observed radial extent of AGN outflows is $\leq$ 1 kpc in most cases, galactic scale outflows, as Totoro would be, given its extreme distance from Satsuki, are also reported (e.g., López-Cobá et al. 2019; Leung et al. 2019; López-Cobá et al. 2020). However, the low gas velocities (Figure 3c and 3d) do not support the scenario of an energetic outflow.

Nonetheless, we should note that although an AGN does not seem like a plausible mechanism for moving Hα or CO out of the galaxy core to the current position of Totoro, the potential cavities identified in Satsuki suggest that in the past (~ 40 Myr ago) the AGN was indeed active and had non-negligible impact on its surroundings (O'Sullivan et al. 2019).

3.3.3. *Gas Ionized by AGN*

There have been studies showing that AGNs are able to ionize gas extending to large distance, such as the

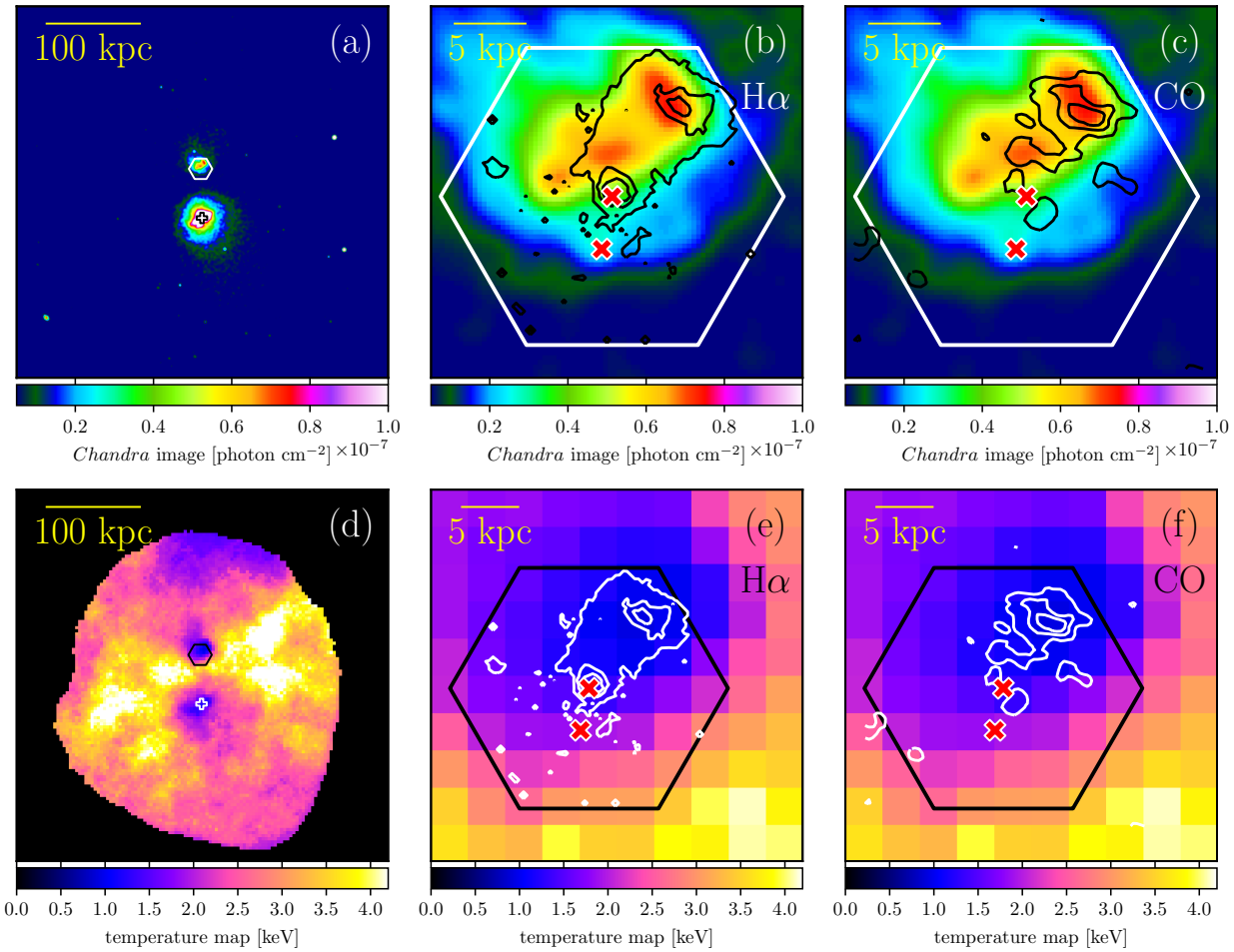

Figure 9. *Chandra* 0.5 – 2 keV maps (a)-(c) and temperature maps (d)-(f) taken from O'Sullivan et al. (2019). In each row, from left to right we show the full map, zoom in on the MaNGA FoV with Hα contours overlaid, and zoom in on the MaNGA FoV with CO contours overlaid. In panel (a) and (d), the nucleus of NGC 6338 is marked by an open cross. The MaNGA hexagonal FoV is also indicated in the figures. In panel (b), (c), (e), and (f), the red filled crosses indicate the nuclei of Satsuki and Mei. The maps show that the Hα and CO emissions are coincident with X-ray structures and low temperature regions.

well-known ionized cloud Hanny's Voorwerp $\sim$ 20 kpc from its host galaxy IC 2497 (e.g., Husemann et al. 2008; Lintott et al. 2009; Husemann et al. 2010). It is believed that an interaction-triggered, currently fading AGN, illuminated and ionized Hanny's Voorewerp (Lintott et al. 2009; Józsa et al. 2009; Keel et al. 2012). Diffuse ionized gas similar to Hanny's Voorewerp was also found $\sim$ 32 kpc north of the iconic interacting galaxies NGC 5194/5195 or M51 (Watkins et al. 2018). The low AGN luminosity and activity and the tidal history provide similarities between Satsuki, IC 2497 and M51.

However, there are also several differences between Hanny's Voorwerp and the M51 cloud and Totoro in terms of excitation state (Seyfert versus LINER-HII, morphology (diffuse for Hanny's Voorwerp and M51's cloud versus centrally-concentrated for Totoro), and the properties of the host galaxy (late type versus early type, see Paper I for the details). For these reasons, we argue that this scenario is unlikely.

3.4. *Cooling Gas*

3.4.1. *Spatial Comparison of Cold, Warm, and Hot Gas*

A scenario we did not consider in Paper I is the cooling of the hot IGM or ICM. Observations of the central regions of some galaxy groups and clusters show strong X-ray emission suggesting that the IGM and ICM are undergoing rapid cooling (e.g., Fabian 1994), and in some cases ionized and molecular gas which are thought to be the product of that cooling (Babyk et al. 2018; Lakhchaura et al. 2018; Olivares et al. 2019; Russell et al. 2019).

O'Sullivan et al. (2019) shows that the X-ray peak of the southern clump in Figure 9a is consistent with the optical centroid of NGC 6338. Three X-ray filaments are observed to extend from the galaxy center, following

the same branching filamentary structure as the Hα gas (Figure 7c). These X-ray filaments are cooler than their surroundings and have very low gas entropies and short cooling times (O'Sullivan et al. 2019), strongly indicating that they are a locus of cooling from the IGM. Young X-ray cavities are also found in NGC 6338, suggesting recent AGN outbursts in this galaxy.

As shown in Figure 9b, the peak of Hα emission (contours) at the nucleus of Satsuki is not associated with the bar, but the position of Totoro corresponds to the brightest X-ray peak. This was first noted by O'Sullivan et al. (2019) who showed that this was also the coolest part of the X-ray bar, and concluded that the Hα was likely material cooled from the IGM, as in the filaments of NGC 6338. They also suggested that the offset between Satsuki and the center of the X-ray clump is evidence that ram-pressure forces caused by the (supersonic) motion of the galaxy are detaching the gas from the galaxy. In this scenario, the X-ray bar would once have been centered on Satsuki, but has been pushed back to the north and perhaps along the line of sight, away from the galaxy core.

Figure 9c shows our CO data overlaid on the *Chandra* image. The molecular gas is well correlated with the western X-ray knot, and (as previously discussed) with the Hα. Figures 9d-e show the *Chandra* temperature maps from O'Sullivan et al. (2019) showing the cool gas around NGC 6338 and Satsuki, and the high-temperature gas between the two, which has been shock-heated by the group-group merger. Overlaid Hα and CO contours show that the ionized and molecular gas are located in the coolest part of the IGM, as in NGC 6338 and the centers of other groups and clusters (e.g., Salomé et al. 2006; Hamer et al. 2012).

3.4.2. *Cooling Time and Gas Properties*

Studies have shown that warm and cold gas in the brightest group and cluster galaxies (BCGs) are preferentially observed in systems where the cooling times lie below $\sim$ 1 Gyr (Edge 2001; Salomé, & Combes 2003; Cavagnolo et al. 2008; Rafferty et al. 2008; Pulido et al. 2018). O'Sullivan et al. (2019) found that the cooling times are as short as <1 Gyr in both cores of Satsuki and NGC 6338. We can also estimate the cooling time around Totoro, i.e., the west end of the X-ray bar as a cylinder of radius 2.8″(1.5 kpc) and length 11.2″ (5.9 kpc, corresponding to the Region 2 in Figure 10b of O'Sullivan et al. 2019). The temperature, density, and luminosity of the X-ray gas are estimated via spectral fitting of the *Chandra* data. Using Equation (1) in O'Sullivan et al. (2019), we estimate the cooling time ($t_{\rm cool}$) in the Totoro region to be $2.2^{+0.2}_{-0.1} \times 10^8$ yr, well within the regime where warm and cold gas are expected.

If the warm and cold gas have indeed cooled from the hot gas, one would expect the hot gas to be significantly more massive than the cool/warm gas. The hot gas mass is derived from a radial deprojected profile (Figure 9 in O'Sullivan et al. 2019), centering on the middle of the X-ray bar. Within a radius of 6.5 kpc, the hot gas mass ($M_{\rm X}$) is $1.2^{+1.07}_{-0.24} \times 10^9$ M$_\odot$. The derived hot gas mass is indeed significantly higher than the total mass of warm ($\sim 10^5$ M$_\odot$ from Hα) and cold gas ($\sim 10^8$ M$_\odot$ from CO).

The ratio of the cold to hot gas of Totoro is $\sim$ 17%. Pulido et al. (2018) investigate the molecular gas properties of 55 central cluster galaxies. They found a strong correlation of hot and cold gas mass traced by X-ray and CO, suggesting that the hot and cold gas arise from the same ensemble of clouds. In other words, the cold gas is unlikely a result of external effects, such as merger or stripping from a plunging galaxy. The average fraction of cold to hot gas in their sample is $\sim$ 18%. The cold to hot gas mass ratio of Totoro is in good agreement with that of these central cluster galaxies (see also Olivares et al. 2019). The consistency provides support that a similar process to that in the central cluster galaxies has occurred in Satsuki and Totoro.

In addition, molecular mass has been found to be correlated with the amount of Hα gas expressed by $L_{\rm H\alpha}$ in the cooling-core galaxies of clusters (Edge 2001; Salomé, & Combes 2003). In Figure 10 we show the H_2 gas mass versus $L_{\rm H\alpha}$ for data taken from the literatures. Totoro is overlaid with a orange square, and falls at the low end of the correlation. The consistency of Totoro with the $M_{\rm H_2}$- $L_{\rm H\alpha}$ relationship of cooling systems again supports a similar process of cooling in the system. To put it another way, our multi-wavelength data of Totoro show that its position on the mass (or luminosity) relations between cold ($\lesssim$ 100 K; CO), warm ($\sim 10^4$ K, Hα), and hot ($> 10^7$ K, X-ray) gas is in line with the gas content of systems with short cooling times. We summarize the physical properties of Totoro in Table 2.

As a side note, the cold and warm gas in cooling systems often appear filamentary, but it is worth noting that the multi-phase gas morphologies of our target are strikingly similar to the BCG of cluster Abell 1991 reported by Hamer et al. (2012) (see their Figure 2). The Hα-emitting gas is relatively circular (blob-like) and is spatially coincident with the most rapidly cooling region (X-ray peak) of the ICM. The peak in the Hα and X-ray gas lies roughly 11 kpc to the north of the BCG, and there are connecting arm structures between the peak and the secondary peak at the galactic nucleus. Moreover, the bulk of the molecular gas with a mass of

$\sim 8\times 10^8$ $M_\odot$ is also found at the location of the cooling region. However, note that spatial resolution must play an important role in detecting the morphology of cooling gas. We cannot rule out that the morphologies of Totoro and the cooling gas in Abell 1991 are more filamentary than a single peak.

Finally, the velocity fields of cooling gas in galaxy clusters, traced by CO and Hα, are characteristic of slow motions (projected velocity < 400 km s^{-1}), narrow line widths (< 250 km s^{-1}) and a lack of relaxed (e.g., rotating) structures (e.g., Salomé et al. 2008; Hamer et al. 2012; Olivares et al. 2019). The observed velocity structures, despite low velocity resolutions, of Totoro traced by CO and Hα (Figures 3c and 3d) agree with that of other cooling systems. In addition, the gas velocities of Totoro traced by CO and Hα are not exactly identical, but the differences are small, ~ 35 km s^{-1} at the main blob region and $60 - 90$ km s^{-1} at the connecting arms. This is also consistent with the finding by Olivares et al. (2019) that the velocity difference between CO and Hα gas is well below 100 km s^{-1}, providing an additional support for CO and Hα gas arising from the same bulk of clouds. The velocity difference may be related to different velocity resolution of CO and Hα observations and line of sight projection effect. We should note again that our CO and Hα observations suffer from low velocity resolutions, therefore the velocity fields must be interpreted with caution. Nonetheless, the maps still provide a guide of the velocity resolution needed for future observation of this system. Future high velocity-resolution CO and Hα observations are required to reveal the detailed gas kinematics of Totoro.

3.4.3. *Environments*

While most of the studies of cooling gas focus on BCGs in rich clusters, cold gas cooling from the hot X-ray medium is also observed at smaller scales in galaxy groups, such as NGC 5044, NGC 4638 and NGC5846 (David et al. 2014; Temi et al. 2018). In fact, the observed cool-core fractions for galaxy groups are slightly higher than those of galaxy clusters (O'Sullivan et al. 2017). Therefore, gas cooled from the IGM is not unique to Totoro.

In Section 3.1, we argue that the cold gas in Totoro is unlikely to be the primitive gas of Satsuki being stripped by ram-pressure. Nonetheless, the X-ray tail (Figure 9a) and the offset between the center of the X-ray bar and the optical centroid of Satsuki are both evidence that the motion of the dry merger (Satsuki and Mei) is rapid enough to lead to stripping of the hot gas halo (O'Sullivan et al. 2019). The question then arises of where and when the ionized and molecular gas we observe was formed; have ram-pressure or other effects changed its location? We might normally expect to see the most rapid cooling in or near the galaxy center. However, the offset of the X-ray bar means that the densest, coolest IGM gas is no longer located at the center of Satsuki. Ram-pressure, by pushing the X-ray halo and bar away from the core of Satsuki, may therefore have caused a reduction in cooling in the galaxy center (O'Sullivan et al. 2019).

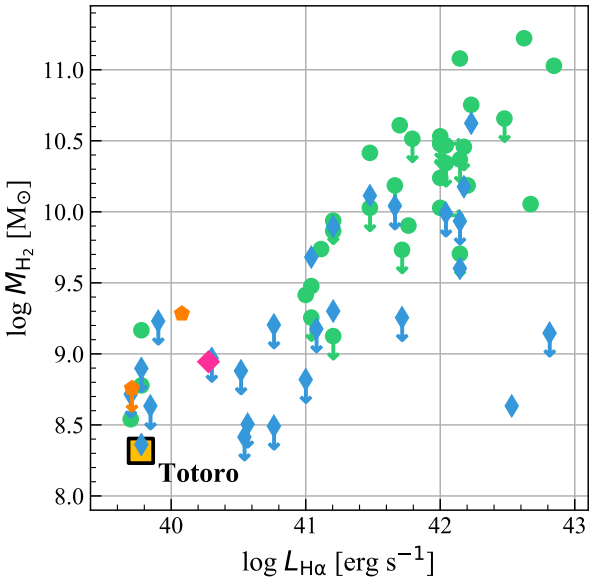

Figure 10. Hα luminosity versus molecular gas mass of cooling gas in cluster galaxies. Data points marked with circles, thin diamonds, pentagons, and diamond are taken from Edge (2001), Salomé, & Combes (2003), McDonald et al. (2012), and Hamer et al. (2012), respectively. Totoro is shown by an orange square and lies on the relationship of other systems.

CO emission occurs in dense molecular clouds which are "self-shielding" from the ionizing effects of the surrounding environment. While some of the Hα emission likely comes from the outer layers of such molecular cloud complexes, observations show that in some cooling systems the Hα emission is considerably more extended than the molecular gas (e.g., in NGC 5044; Schellenberger et al. 2020) which may suggest it is associated with a less dense cooled gas component. Such low-density material would likely move with the surrounding IGM if ram-pressure pushed it back from the galaxy. Dense molecular clouds would not be affected by ram-pressure, and might be expected to fall under gravity toward the center of Satsuki, unless they are connected to the IGM via magnetic fields (McCourt et al. 2015) or surrounding layers of neutral and ionized gas (Li et al. 2018). Even with such connections to the surrounding environment, it seems implausible that the

molecular gas could have condensed out of the IGM in the core of Satsuki and then been uplifted. The correlation between the CO, Hα and the coolest X-ray gas strongly suggests that the molecular and ionized gas is the product of cooling from the IGM at its current location, i.e., that cooling has occurred (and may be ongoing) in Totoro, well outside the center of Satsuki.

Last but not least, as suggested by O'Sullivan et al. (2019) and this work, we are witnessing a merger between two groups undergoing rapid radiative cooling. Further analysis on the multi-wavelength phase of cooling gas in NGC 6338, from cold to hot gas as in this study, will be carried in a separate paper (O'Sullivan et al. in preparation).

3.4.4. *Future of the Gas*

Cooling gas can potentially serve as the fuel for an AGN and/or central star formation (O'Dea et al. 2008; Rafferty et al. 2008; Mittal et al. 2009; Hicks et al. 2010; Fogarty et al. 2017). In X-ray bright groups, like our target, star formation in the central galaxy is generally weak even in systems known to be cooling. By contrast, as many as 85 – 90% of group-dominant galaxies have radio AGN, moreover, dominant galaxies with active or recently active radio jets are relatively common in X-ray bright groups (Kolokythas et al. 2018, 2019). Galaxy cluster-dominant galaxies, however, seem much more likely to have significant star formation.

Here we consider whether the cooling gas would fuel star formation assuming the gas will fall back into Satsuki. McDonald et al. (2018) compare the cooling rate of the ICM/IGM to the observed SFR in the central galaxy for a sample of isolated ellipticals, groups, and clusters. They found that the cooling ICM/IGM is not providing the fuel for star formation in systems with cooling rate < 30 M$_\odot$ yr^{-1}, which are dominated by groups and isolated ellipticals. On the other hand, SFR increases with increasing cooling rate for the rapidly cooling systems (> 30 M$_\odot$ yr^{-1}), presumably due to an increase in either the cooling efficiency of the hot gas or the star formation efficiency of the cooled gas (see also Edge 2001; Salomé, & Combes 2003; O'Dea et al. 2008). The cooling rate ($M_{\rm X}/t_{\rm cool}$) of Totoro is $\sim 1.2 \times 10^9$ M$_\odot$/2.2×10^8 yr ≈ 5 M$_\odot$ yr^{-1}. In this aspect, the cooling gas in our group-dominant, relatively low cooling-rate system is less likely to significantly contribute to star formation.

Moreover, star formation can be suppressed by AGN feedback even in systems with short cooling times. The summed AGN jet power ($P_{\rm cav}$) for both cavities associated with Satsuki from O'Sullivan et al. (2019) is (0.97 – 2.67) $\times 10^{41}$ erg s^{-1} (an estimate of heating; the actual value depends on the cavity age used: buoyant rise time, sonic expansion time-scale, or refill time), the energy is comparable to the X-ray luminosity for the whole X-ray emitting gas ($\sim 3 \times 10^{41}$ erg s^{-1}; an estimate of cooling). Rafferty et al. (2008) find a tendency for star-forming systems to have low $P_{\rm cav}/L_X$ ratios (< 1) and quiescent systems to have high $P_{\rm cav}/L_X$ ratios (> 1), supporting the suppression of star formation by AGN feedback. However, this is not exclusively the case; star-forming cooling systems can have high $P_{\rm cav}/L_X$ ratios, and vice versa. The estimated heating available from the cavities around Satsuki make it a borderline case, and the ongoing merger and stripping add to the complexities. The fate of Totoro may depend on how effectively energy from the cavities can heat their surroundings.

Finally, it is worth mentioning that Satsuki and Totoro may host a little star-formation activity with an upper limit of < 0.059 and < 0.047 M$_\odot$ yr^{-1}, respectively, assuming all the Hα fluxes come from star formation. It is unclear if the current star formation (if any) is related to the cooling and gas fueling processes. McDonald et al. (2018) attribute the low-level star formation in low cooling rate systems to recycling of gas lost by evolved stars, namely, the star formation is not related to cooling gas.

4. SUMMARY

In Paper I, we identified an Hα blob Totoro ~ 8 kpc away from a dry merger (Satsuki and Mei) from MaNGA data (Figure 1). Here we present new optical (wide-field Hα and u-band), millimeter (^{12}CO(1-0)) observations, and published X-ray data (O'Sullivan et al. 2019), with the aim of providing significant constraints and answers to fundamental questions regarding the nature of Totoro. The main conclusions of this paper are as follows:

- The data disfavor the scenario that Totoro is stripped from Satsuki by ram-pressure based on the morphology and kinematics of ionized (Hα) and molecular gas) and the properties of the host galaxy (Section 3.1 and Figure 3).

We consider whether Totoro is a separate galaxy interacting with the dry merger (Satsuki and Mei) from several aspects:

- We apply three commonly-used methods to g-, r-, and i-band images (Figure 4) to look for an underlying stellar counterpart of Totoro. However, we find no compact underlying stellar component associated with Totoro (Section 3.2.1 and Figure 5).

- No tidal tail feature is seen in Hα beyond the MaNGA FoV. If Totoro is a galaxy interacting

with the dry merger (Satsuki and Mei), it may have a non-typical tidal history and morphology, or it is a completely disrupted low-surface-brightness dwarf galaxy (Section 3.2.2, Figure 7 and Table 3).

- However, Totoro shows different star formation, gas, and dust properties (in terms of M_{H_2}-SFR, Σ_*-$\Sigma_{H\alpha}$, and A_V-Σ_{SFR} relations and gas kinematics) from that of a variety of nearby galaxy populations (i.e., star-forming and quiescent galaxies, low-surface-brightness and ultra-diffuse galaxies). Therefore, Totoro is unlikely to be a separate galaxy interacting with the dry merger (Satsuki and Mei) (Section 3.2.3 and Figure 8).

- The u-band data, which are sensitive to recent star formation, show no strong sign of recent star formation at the position of Totoro. Therefore, the ionized gas of Totoro is unlikely to be powered by star formation, confirming the results of emission line ratios diagnostics in Paper I and previous bullet-point that Totoro is not an analogue of a star-forming region in nearby galaxy populations (Section 3.2.1 and Figure 5).

We consider whether Totoro is a result of AGN activity.

- However, in spite of possible past AGN outbursts, the multi-wavelength data show no direct evidence for an active ongoing AGN in Satsuki or Mei. Moreover, Totoro is unlikely to be gas being ionized or ejected by an AGN as its physical properties (gas excitation state, morphology, and kinematics, etc.) are distinct from similar objects (Section 3.3).

Finally, we consider whether Totoro is formed via cooling of hot IGM as implied by O'Sullivan et al. (2019).

- We compare the spatial distribution of Hα and CO with X-ray intensity and temperature maps. We find that the ionized and molecular gas are related to the most rapidly cooling region of the hot IGM. The cooling time in the Totoro region is well within the regime where cooling is expected (Section 3.4.1 and 3.4.2 and Figure 9).

- The mass (or luminosity) relations between cold (< 100 K; CO), warm ($\sim 10^4$ K, Hα), and hot ($> 10^7$ K, X-ray) gas, as well as gas kinematics are in line with the gas content of cooling systems, supporting again that Totoro originates from the same physical process of cooling gas (Section 3.4.2 and Figure 10).

- Previous study by O'Sullivan et al. (2019) suggests that the densest, coolest X-ray gas has been pushed away from the core of the host galaxy Satsuki by ram-pressure. The correlation between the CO, Hα and the coolest X-ray gas presented in this work strongly suggests that the molecular and ionized gas is the product of cooling from the hot X-ray gas and is formed at its current location, leading to the observed *offset* cooling and the reduction in cooling in the galaxy core (Section 3.4.3).

- The cooling rate of Totoro is considerably lower than that of star-forming cooling systems. The estimated heating available from the cavities around Satsuki is comparable to the cooling X-ray luminosity. The fate of Totoro may depend on how effectively energy from the cavities can heat their surroundings, but note that the ongoing merger (Satsuki, Mei, and NGC 6338) and stripping add to the complexities (Section 3.4.4).

In the majority of clusters the peaks of optical and X-ray emission are very close to the center of galaxy, so it is difficult to determine whether the appearances of warm or even cold gas are primarily related to the cooling of the IGM/ICM or the host galaxy. Offset cooling is rare ($< 5\%$, e.g., Hamer et al. 2012), therefore VII Zw 700 provides an exceptional opportunity to constrain the gas cooling process and the interplay between cooling gas and host galaxy. In future work, we intend to constrain the gas kinematics at the connecting arms with high-spectral-resolution data to quantify the potential of a fueling process for Satsuki. A detailed multi-wavelength analysis, from CO to Hα, to other optical lines (e.g., Hβ, [NII], [OIII], etc.), and to X-ray, will be presented in an upcoming paper (O'Sullivan et al in preperation). Moreover, the large sample of optical IFU survey MaNGA ($\sim$ 5,000 galaxies in the latest SDSS data releases DR15/16 and $\sim$ 10,000 in the future) along with the *Chandra* archive is a suitable starting point for future multi-wavelength statistical studies of cooling gas properties. Although MaNGA does not target specific environments, the large sample size of MaNGA ensures observations of numerous galaxies located in groups and clusters. Given the significant fraction of cooling cores in galaxy clusters/groups (e.g., Mittal et al. 2009; O'Sullivan et al. 2017), more cooling gas candidates are expected in the final MaNGA sample.

ACKNOWLEDGMENTS

We would like to thank the anonymous referee for constructive comments that helped to improve the manuscript. H.A.P thanks Eva Schinnerer, Christine Wilson, and Toshiki Saito for useful discussions. This work is supported by the Academia Sinica under the Career Development Award CDA-107-M03 and the Ministry of Science & Technology of Taiwan under the grant MOST 108-2628-M-001-001-MY3. M.J.M. acknowledges the support of the National Science Centre, Poland through the SONATA BIS grant 2018/30/E/ST9/00208, the Royal Society of Edinburgh International Exchange Programme, and the hospitality of the Academia Sinica Institute of Astronomy and Astrophysics (ASIAA). EOS gratefully acknowledges the support for this work provided by the National Aeronautics and Space Administration(NASA) through *Chandra* Award Number G07-18162X, issued by the *Chandra* X-ray Center, which is operated by the Smithsonian Astrophysical Observatory for and on behalf of NASA under contract NAS8-03060. SFS is grateful for the support of a CONACYT grant FC-2016-01-1916, and funding from the PAPIIT-DGAPA-IN100519 (UNAM) project. J.G.F-T is supported by FONDECYT No. 3180210 and Becas Iberoamérica Investigador 2019, Banco Santander Chile.

This project makes use of the MaNGA-Pipe3D dataproducts (Sánchez et al. 2016b, 2018). We thank the IA-UNAM MaNGA team for creating this catalogue, and the Conacyt Project CB-285080 for supporting them.

This work is partly based on observations carried out under project number S16BE001 with the IRAM NOEMA Interferometer. IRAM is supported by INSU/CNRS (France), MPG (Germany) and IGN (Spain).

This work is partly based on observations obtained with MegaPrime/MegaCam, a joint project of CFHT and CEA/DAPNIA, at the Canada-France-Hawaii Telescope (CFHT) which is operated by the National Research Council (NRC) of Canada, the Institut National des Sciences de l'Univers of the Centre National de la Recherche Scientifique of France, and the University of Hawaii. The authors also wish to recognize and acknowledge the very significant cultural role and reverence that the summit of Maunakea has always had within the indigenous Hawaiian community. We are most fortunate to have the opportunity to conduct observations from this mountain.

This work is partly based on observations obtained with the 6-m telescope of the Special Astrophysical Observatory of the Russian Academy of Sciences carried out with the financial support of the Ministry of Science and Higher Education of the Russian Federation (including agreement No. 05.619.21.0016, project ID RFMEFI61919X0016). The analysis of the ionized gas distribution according SCORPIO-2 data was supported by the grant of Russian Science Foundation project 17-12-01335 "Ionized gas in galaxy discs and beyond the optical radius".

This work use GAIA to derive aperture photometry. GAIA is a derivative of the SKYCAT catalogue and image display tool, developed as part of the VLT project at ESO. SKYCAT and GAIA are free software under the terms of the GNU copyright. The 3D facilities in GAIA use the VTK library.

This research made use of APLpy, an open-source plotting package for Python (Robitaille, & Bressert 2012).

Funding for the Sloan Digital Sky Survey IV has been provided by the Alfred P. Sloan Foundation, the U.S. Department of Energy Office of Science, and the Participating Institutions. SDSS-IV acknowledges support and resources from the Center for High-Performance Computing at the University of Utah. The SDSS web site is www.sdss.org.

SDSS-IV is managed by the Astrophysical Research Consortium for the Participating Institutions of the SDSS Collaboration including the Brazilian Participation Group, the Carnegie Institution for Science, Carnegie Mellon University, the Chilean Participation Group, the French Participation Group, Harvard-Smithsonian Center for Astrophysics, Instituto de Astrofísica de Canarias, The Johns Hopkins University, Kavli Institute for the Physics and Mathematics of the Universe (IPMU) / University of Tokyo, the Korean Participation Group, Lawrence Berkeley National Laboratory, Leibniz Institut für Astrophysik Potsdam (AIP), Max-Planck-Institut für Astronomie (MPIA Heidelberg), Max-Planck-Institut für Astrophysik (MPA Garching), Max-Planck-Institut für Extraterrestrische Physik (MPE), National Astronomical Observatories of China, New Mexico State University, New York University, University of Notre Dame, Observatário Nacional / MCTI, The Ohio State University, Pennsylvania State University, Shanghai Astronomical Observatory, United Kingdom Participation Group, Universidad Nacional Autónoma de México, University of Arizona, University of Colorado Boulder, University of Oxford, University of Portsmouth, University of Utah, University of Virginia, University of Washington, University of Wisconsin, Vanderbilt University, and Yale University.

REFERENCES

Afanasiev, V. L., & Moiseev, A. V. 2011, Baltic Astronomy, 20, 363

Aguado, D. S., Ahumada, R., Almeida, A., et al. 2019, ApJS, 240, 23

Amorisco, N. C., & Loeb, A. 2016, Monthly Notices of the Royal Astronomical Society, 459, L51

Babyk, I. V., McNamara, B. R., Nulsen, P. E. J., et al. 2018, ApJ, 857, 32

Baldwin, J. A., Phillips, M. M., & Terlevich, R. 1981, PASP, 93, 5

Balogh, M. L., Baldry, I. K., Nichol, R., et al. 2004, ApJL, 615, L101

Barazza, F. D., Binggeli, B., & Jerjen, H. 2002, A&A, 391, 823

Barbary, K. 2016, The Journal of Open Source Software, 1,58, doi: 10.21105/joss.00058

Bellhouse, C., Jaffé, Y. L., Hau, G. K. T., et al. 2017, ApJ, 844, 49

Bellhouse, C., Jaffé, Y. L., McGee, S. L., et al. 2019, MNRAS, 485, 1157

Bertin, E., & Arnouts, S. 1996, A&AS, 117, 393

Bílek, M., Cuillandre, J.-C., Gwyn, S., et al. 2016, A&A, 588, A77

Blanton, M. R., & Roweis, S. 2007, AJ, 133, 734

Blanton, M. R., Bershady, M. A., Abolfathi, B., et al. 2017, AJ, 154, 28

Bohlin, R. C., Savage, B. D., & Drake, J. F. 1978, ApJ, 224, 132

Bolatto, A. D., Wolfire, M., & Leroy, A. K. 2013, ARA&A, 51, 207

Bond, J. R., Cole, S., Efstathiou, G., et al. 1991, ApJ, 379, 440

Boselli, A., Cuillandre, J. C., Fossati, M., et al. 2016, A&A, 587, A68

Brammer, G. B., van Dokkum, P. G., & Coppi, P. 2008, ApJ, 686, 1503

Brammer, G. B., Whitaker, K. E., van Dokkum, P. G., et al. 2009, ApJL, 706, L173

Bundy, K., Bershady, M. A., Law, D. R., et al. 2015, ApJ, 798, 7

Calette, A. R., Avila-Reese, V., Rodríguez-Puebla, A., et al. 2018, RMxAA, 54, 443

Cao, T.-W., Wu, H., Du, W., et al. 2017, AJ, 154, 116

Cavagnolo, K. W., Donahue, M., Voit, G. M., et al. 2008, ApJL, 683, L107

Cherinka, B., Andrews, B. H., Sánchez-Gallego, J., et al. 2019, AJ, 158, 74

Colbert, J. W., Mulchaey, J. S., & Zabludoff, A. I. 2001, AJ, 121, 808

Consolandi, G., Gavazzi, G., Fossati, M., et al. 2017, A&A, 606, A83

David, L. P., Lim, J., Forman, W., et al. 2014, ApJ, 792, 94

Di Cintio, A., Brook, C. B., Dutton, A. A., et al. 2017, Monthly Notices of the Royal Astronomical Society, 466, L1

Dopita, M. A., Kewley, L. J., Sutherland, R. S., et al. 2016, Ap&SS, 361, 61

Drory, N., MacDonald, N., Bershady, M. A., et al. 2015, AJ, 149, 77

Duc, P.-A., Cuillandre, J.-C., Karabal, E., et al. 2015, MNRAS, 446, 120

Edge, A. C. 2001, MNRAS, 328, 762

Egami, E., Misselt, K. A., Rieke, G. H., et al. 2006, ApJ, 647, 922

Ellison, S. L., Patton, D. R., Simard, L., et al. 2008, AJ, 135, 1877

Evans, N. J., Dunham, M. M., Jørgensen, J. K., et al. 2009, ApJS, 181, 321

Fabian, A. C. 1994, ARA&A, 32, 277

Fernández-Trincado, J. G., Forero-Romero, J. E., Foex, G., et al. 2014, ApJL, 787, L34

Fioc, M., & Rocca-Volmerange, B. 1997, A&A, 326, 950

Fogarty, K., Postman, M., Larson, R., et al. 2017, ApJ, 846, 103

Gomes, J. M., Papaderos, P., Kehrig, C., et al. 2016, A&A, 588, A68

Grazian, A., Fontana, A., de Santis, C., Nonino, M., Salimbeni, S., Giallongo, E., Cristiani, S., Gallozzi, S., et al. 2006, A&A, 449, 951

Gu, M., Ho, L. C., Peng, C. Y., et al. 2013, ApJ, 773, 34

Gunn, J. E., & Gott, J. R. 1972, ApJ, 176, 1

Gwyn, S. D. J. 2008, PASP, 120, 212

Hamer, S. L., Edge, A. C., Swinbank, A. M., et al. 2012, MNRAS, 421, 3409

Hao, C. N., Mao, S., Deng, Z. G., et al. 2006, MNRAS, 370, 1339

Hicks, A. K., Mushotzky, R., & Donahue, M. 2010, ApJ, 719, 1844

Hopkins, P. F., Hernquist, L., Cox, T. J., et al. 2008, ApJS, 175, 356

Hsieh, B. C., Lin, L., Lin, J. H., et al. 2017, ApJL, 851, L24

Huang, S., Leauthaud, A., Greene, J. E., et al. 2018, MNRAS, 475, 3348

Husemann, B., Wisotzki, L., Sánchez, S. F., et al. 2008, A&A, 488, 145

Husemann, B., Sánchez, S. F., Wisotzki, L., et al. 2010, A&A, 519, A115

Jáchym, P., Kenney, J. D. P., Sun, M., et al. 2019, ApJ, 883, 145
Józsa, G. I. G., Garrett, M. A., Oosterloo, T. A., et al. 2009, A&A, 500, L33
Keel, W. C., Lintott, C. J., Schawinski, K., et al. 2012, AJ, 144, 66
Kennicutt, R. C. 1989, ApJ, 344, 685
Kennicutt, R. C. 1998, ApJ, 498, 541
Kim, T., Sheth, K., Hinz, J. L., et al. 2012, ApJ, 753, 43
Kolokythas, K., O'Sullivan, E., Raychaudhury, S., et al. 2018, MNRAS, 481, 1550
Kolokythas, K., O'Sullivan, E., Intema, H., et al. 2019, MNRAS, 489, 2488
Lacey, C., & Cole, S. 1993, MNRAS, 262, 627
Lakhchaura, K., Werner, N., Sun, M., et al. 2018, MNRAS, 481, 4472
Lang, D., Hogg, D. W., Mierle, K., et al. 2010, AJ, 139, 1782
Larson, R. B., & Tinsley, B. M. 1978, ApJ, 219, 46
Law, D. R., Yan, R., Bershady, M. A., et al. 2015, AJ, 150, 19
Law, D. R., Cherinka, B., Yan, R., et al. 2016, AJ, 152, 83
Lee, B., & Chung, A. 2018, ApJL, 866, L10
Leung, G. C. K., Coil, A. L., Aird, J., et al. 2019, ApJ, 886, 11
Li, Y., Ruszkowski, M., & Tremblay, G. 2018, ApJ, 854, 91
Li, H., Wuyts, S., Lei, H., et al. 2019, ApJ, 872, 63
Lin, L., Lin, J.-H., Hsu, C.-H., et al. 2017, ApJ, 837, 32
Lintott, C. J., Schawinski, K., Keel, W., et al. 2009, MNRAS, 399, 129
López-Cobá, C., Sánchez, S. F., Bland-Hawthorn, J., et al. 2019, MNRAS, 482, 4032
López-Cobá, C., Sánchez, S. F., Anderson, J. P., et al. 2020, AJ, 159, 167
Mantha, K. B., McIntosh, D. H., Ciaschi, C. P., et al. 2019, MNRAS, 486, 2643
Martel, A. R., Ford, H. C., Bradley, L. D., et al. 2004, AJ, 128, 2758
Matthews, L. D., Gao, Y., Uson, J. M., et al. 2005, The Astronomical Journal, 129, 1849
McCourt, M., O'Leary, R. M., Madigan, A.-M., et al. 2015, MNRAS, 449, 2
McDonald, M., Wei, L. H., & Veilleux, S. 2012, ApJL, 755, L24
McDonald, M., Gaspari, M., McNamara, B. R., et al. 2018, ApJ, 858, 45
McGaugh, S. S., Schombert, J. M., & Lelli, F. 2017, ApJ, 851, 22
Mihos, J. C. 2004, Recycling Intergalactic and Interstellar Matter, 390
Mittal, R., Hudson, D. S., Reiprich, T. H., et al. 2009, A&A, 501, 835
Moustakas, J., Kennicutt, R. C., & Tremonti, C. A. 2006, ApJ, 642, 775
O'Dea, C. P., Baum, S. A., Privon, G., et al. 2008, ApJ, 681, 1035
Oh, S., Greene, J. E., & Lackner, C. N. 2017, ApJ, 836, 115
Olivares, V., Salome, P., Combes, F., et al. 2019, A&A, 631, A22
O'Neil, K., Schinnerer, E., & Hofner, P. 2003, The Astrophysical Journal, 588, 230
O'Sullivan, E., Ponman, T. J., Kolokythas, K., et al. 2017, MNRAS, 472, 1482
O'Sullivan, E., Schellenberger, G., Burke, D. J., et al. 2019, MNRAS, 488, 2925
Pan, H.-A., Lin, L., Hsieh, B.-C., et al. 2018, ApJ, 854, 159
Pandge, M. B., Vagshette, N. D., David, L. P., et al. 2012, MNRAS, 421, 808
Peng, C. Y., Ho, L. C., Impey, C. D., et al. 2010, AJ, 139, 2097
Poggianti, B. M., Moretti, A., Gullieuszik, M., et al. 2017, ApJ, 844, 48
Prescott, M., Baldry, I. K., & James, P. A. 2009, MNRAS, 397, 90
Pulido, F. A., McNamara, B. R., Edge, A. C., et al. 2018, ApJ, 853, 177
Rafferty, D. A., McNamara, B. R., & Nulsen, P. E. J. 2008, ApJ, 687, 899
Rahman, N., Bolatto, A. D., Wong, T., et al. 2011, ApJ, 730, 72
Roberts-Borsani, G. W. 2020, MNRAS, 494, 4266
Robitaille, T., & Bressert, E. 2012, APLpy: Astronomical Plotting Library in Python, ascl:1208.017
Rubin, D., Hayden, B., Huang, X., et al. 2018, ApJ, 866, 65
Russell, H. R., McNamara, B. R., Fabian, A. C., et al. 2019, MNRAS, 490, 3025
Saintonge, A., Catinella, B., Tacconi, L. J., et al. 2017, ApJS, 233, 22
Salomé, P., & Combes, F. 2003, A&A, 412, 657
Salomé, P., Combes, F., Edge, A. C., et al. 2006, A&A, 454, 437
Salomé, P., Combes, F., Revaz, Y., et al. 2008, A&A, 484, 317
Sánchez, S. F., Kennicutt, R. C., Gil de Paz, A., et al. 2012, A&A, 538, A8
Sánchez, S. F., Pérez, E., Sánchez-Blázquez, P., et al. 2016, RMxAA, 52, 21
Sánchez, S. F., Pérez, E., Sánchez-Blázquez, P., et al. 2016, RMxAA, 52, 171

Sánchez, S. F., Avila-Reese, V., Hernandez-Toledo, H., et al. 2018, RMxAA, 54, 217

Schellenberger, G., David, L. P., Vrtilek, J., et al. 2020, ApJ, 894, 72

Silk, J., & Rees, M. J. 1998, A&A, 331, L1

Singh, R., van de Ven, G., Jahnke, K., et al. 2013, A&A, 558, A43

Sitnik, T. G., Egorov, O. V., Lozinskaya, T. A., et al. 2015, MNRAS, 454, 2486

Springel, V., Di Matteo, T., & Hernquist, L. 2005, ApJL, 620, L79

Steinhauser, D., Haider, M., Kapferer, W., et al. 2012, A&A, 544, A54

Steinhauser, D., Schindler, S., & Springel, V. 2016, A&A, 591, A51

Strateva, I., Ivezić, Ž., Knapp, G. R., et al. 2001, AJ, 122, 1861

Struck, C., & Smith, B. J. 2012, MNRAS, 422, 2444

Tal, T., van Dokkum, P. G., Nelan, J., et al. 2009, AJ, 138, 1417

Taylor, E. N., Hopkins, A. M., Baldry, I. K., et al. 2015, MNRAS, 446, 2144

Temi, P., Amblard, A., Gitti, M., et al. 2018, ApJ, 858, 17

Tody, D. 1986, Proc. SPIE, 627, 733

Tody, D. 1993, Astronomical Data Analysis Software and Systems II, 52, 173

Urry, C. M., & Padovani, P. 1995, PASP, 107, 803

van Dokkum, P. G., Abraham, R., Merritt, A., et al. 2015, The Astrophysical Journal, 798, L45

Vantyghem, A. N., McNamara, B. R., Edge, A. C., et al. 2017, ApJ, 848, 101

Vogt, F. P. A., Dopita, M. A., & Kewley, L. J. 2013, ApJ, 768, 151

Wake, D. A., Bundy, K., Diamond-Stanic, A. M., et al. 2017, AJ, 154, 86

Wang, Y., Lui, F., Shen, Z., et al. 2019, ApJ, 870, 132

Watkins, A. E., Mihos, J. C., Bershady, M., et al. 2018, ApJL, 858, L16

Westfall, K. B., Cappellari, M., Bershady, M. A., et al. 2019, arXiv:1901.00856

Whitaker, K. E., van Dokkum, P. G., Brammer, G., et al. 2012, ApJL, 754, L29

Yozin, C., & Bekki, K. 2015, Monthly Notices of the Royal Astronomical Society, 452, 937

Zhou, Z., Zhou, X., Wu, H., et al. 2017, ApJ, 835, 70